Available online at www.sciencedirect.com
ScienceDirect
Journal of Power Sources 163 (2006) 294–299
JOURNAL OF POWER SOURCES
www.elsevier.com/locate/jpowsour

Short communication

Synthesis of electrode materials by reduction of $KMnO_4$ with $NiCl_2{\cdot}6H_2O$ in aqueous solutions

S.H. Kim, S.J. Kim, J. Kim *

Department of Materials Science and Engineering, Chonnam National University, 300 Yongbong-dong, Buk-ku, Gwangju 500-757, South Korea

Received 8 August 2005; received in revised form 9 June 2006; accepted 28 June 2006
Available online 28 August 2006

Abstract

The nickel–manganese compounds were synthesized by redox reactions in aqueous solutions using potassium permanganate as an oxidizing agent at ambient temperature. Also, a layered Li–Ni–Mn–O system was synthesized by using a nickel–manganese compound as precursor for electrode materials. X-ray diffraction patterns of the lithiated $Li_{1.296}Ni_{0.056}Mn_{0.648}O_2$ sample were indexed to a layered structure based on hexagonal α-$NaFeO_2$ (space group: *R*-3*m*, 166) with signs of monoclinic-related peaks indicating the existence of monoclinic Li_2MnO_3 phase. The lithiated $Li_{1.296}Ni_{0.056}Mn_{0.648}O_2$ electrode provides the initial discharge capacity of 108 mAh g^{-1} and the maximum discharge capacity of 192 mAh g^{-1} between 2.0 and 4.8 V versus Li/Li^+ at 0.2 mA cm^{-2}.

Keywords: Lithium batteries; Nickel–manganese; Redox reactions; Li_2MnO_3; Electrode

1. Introduction

Transition metal oxides are commonly synthesized by repeated grinding and firing at elevated temperatures of the reactants. The higher firing temperature is required to overcome the diffusional limitations associated with limitations size of the reactant particles. Such a high-temperature procedure gives the larger particle size and inhomogeneity and these difficulties have prompted materials chemists to design and develop synthesis methods that can lower the processing temperatures [1,2]. Therefore, several low-temperature methods have attracted much attention in recent years in order to improve various kinds of performances [3–5]. Especially, the low-temperature methods lead to smaller and uniform particle size, which may be beneficial for electrodes materials development efforts in lithium batteries.

Layered lithium manganese oxides are of interest as an alternative cathodic material due to their high specific energy, nontoxicity and low cost. Unfortunately, those layered manganese materials transform to the spinel-like phases by Jahn–Teller distortion during electrochemical cycling. This transformation usually leads to poor rate performance and to steps in the voltage profile [6–8]. To overcome this problem, a number of research groups have studied for increasing the structural stability of lithium manganese oxides by using a concept of a solid solution or nano-composite of $LiMO_2$ (M = Ni, Co, Cr) and Li_2MnO_3 [9–12]. Although whether the concept of a solid-solution or a nano-composite formation for the $LiMO_2$–Li_2MnO_3 system is still in debate, $Li[Ni_xLi_{(1/3-2x/3)}Mn_{(2/3-x/3)}]O_2$ of them seems to be a promising candidate as cathodic material for lithium batteries. The $Li[Ni_xLi_{(1/3-2x/3)}Mn_{(2/3-x/3)}]O_2$ compounds exhibit the thermal stability and good electrochemical performance [13–15]. Lu et al. reported the layered $Li[Ni_xLi_{(1/3-2x/3)}Mn_{(2/3-x/3)}]O_2$ ($0 \leq \times \leq 1/2$) compounds prepared by the "mixed hydroxide" method. $Li[Ni_xLi_{(1/3-2x/3)}Mn_{(2/3-x/3)}]O_2$ with $x = 1/3$ shows a capacity of 200 mAh g^{-1} at 30 °C and a capacity of 220 mAh g^{-1} at 50 °C. Its good electrochemical performance and cycleability are assumed that all Ni^{2+} is oxidized to Ni^{4+} when Li is extracted from $Li[Ni_xLi_{(1/3-2x/3)}Mn_{(2/3-x/3)}]O_2$ while maintains its structural stability by utilize rigid Li_2MnO_3 as a framework [13]. Recently, many research groups have investigated on the role of Li_2MnO_3 framework since Thackeray et al. and Bruce et al. revealed that the electrochemically inactive Li_2MnO_3 could be

* Corresponding author. Tel.: +82 62 530 1703; fax: +82 62 530 1699.
E-mail address: jaekook@chonnam.ac.kr (J. Kim).

0378-7753/$ – see front matter © 2006 Elsevier B.V. All rights reserved.
doi:10.1016/j.jpowsour.2006.06.080

Table 1
The results of inductively coupled plasma (ICP) of as-prepared samples

Sample	Reactant	PH	Element	Weight percentage (%)	Molar ratio
A (adding HCl)	$NiCl_2{\cdot}6H_2O$ $KMnO_4$	1	Ni Mn	5.23 56.82	$Ni_{0.089}Mn_{1.034}$
B (adding KOH)	$NiCl_2{\cdot}6H_2O$ $KMnO_4$	11	Ni Mn	47.61 20.4	$Ni_{0.811}Mn_{0.371}$

activated by acid treatment or by charging it to a high potential [16–19].

In this work, the nickel–manganese compounds were synthesized by redox reactions in aqueous solutions using potassium permanganate as oxidizing agents at ambient temperature. The prepared particles were used as a precursor for electrode materials by lithiation with lithium hydroxide. $Li_{1.296}Ni_{0.056}Mn_{0.648}O_2$ material was prepared and its electrochemical characteristics were investigated. It is particularly interesting to observe a stable electrochemical performance of $Li_{1.296}Ni_{0.056}Mn_{0.648}O_2$ material since it has almost identical stoichiometry and crystalline characteristics to Li_2MnO_3, which has been known as an electrochemically inactive material.

2. Experimental

The nickel–manganese compounds were synthesized by reacting an aqueous solution of nickel chloride with potassium permanganate as oxidizing agent by two different conditions (adding HCl or KOH). In one condition, by using a burette a 50 mL aqueous solution of a 0.5 M $NiCl_2{\cdot}6H_2O$ and a 50 mL aqueous solution of a 0.5 M HCl were dropped slowly into 50 mL of a 0.5 M $KMnO_4$ solutions that was stirred constantly with a magnetic stirrer. In another condition, a 50 mL aqueous solution of a 0.5 M KOH substituting HCl was put into 50 mL of a 0.5 M $KMnO_4$ solutions by using a burette. The precipitate formed after 1 day of reaction was filtered, washed several times with distilled water to remove other reaction products. The precipitates were then dried in an oven at 100 °C for 6 h. To investigate the electrochemical activity of Li_2MnO_3, the as-prepared sample obtained by adding HCl was selected and lithiated. In accordance to the ICP result of the as-prepared samples (Table 1), the as-prepared sample A was mixed with the stoichiometric amount of $Li(OH){\cdot}2H_2O$ and ground. The mixture was palletized and heated in air at 800 °C for 3 h and quenched to room temperature.

The crystalline nature and morphologies of the products were characterized by X-ray powder diffraction (XRD), and field emission scanning electron microscope (FESEM). The structural characterization of the synthesized samples was carried out with X-ray powder diffraction. The X-ray patterns were recorded with a counting degree of 2.00 deg min^{-1} in 2θ range from 10° to 80° by using a Rigaku D/MAX UltimaIII High Resolution X-ray diffractometer (Cu Kα radiation, wave length 1.5406 Å). The morphology and particle size of the samples were characterized with S-4700 FESEM. The chemical composition of the as-prepared samples was determined by inductively coupled plasma (ICP) using a Perkin-Elmer 4300 DV analyzer.

For electrochemical measurements, lithium-inserted materials were mixed with a carbon black and PTFE binder. This mixture were pressed onto a stainless steel mesh and dried under vacuum at 180 °C for 5 h. The cell consisted of a cathode and lithium metal anode separated by a glass fiber. The used electrolyte was a 1:1 mixture of ethylene carbonate (EC) and dimethyl carbonate (DMC) containing 1 M $LiPF_6$. The cells were assembled in a glove box under argon atmosphere and tested between 2.0 and 4.8 V versus Li/Li^+ at 0.2 mA cm^{-2} by using Battery Tester System 2004.

3. Results and discussion

Fig. 1 shows the X-ray diffraction patterns of the samples obtained by reacting an aqueous solution of nickel chloride with potassium permanganate as oxidizing agent. The as-prepared samples show no discernible reflections in the X-ray powder diffraction pattern since those samples were synthesized by redox reactions in aqueous solutions at room temperature as shown in Fig. 1(a) and (c). To characterize the crystal structure, X-ray powder diffraction patterns were also recorded after firing at 500 °C for 6 h. The X-ray patterns of the fired sample A show the existence of the two phases corresponding to tetragonal α-MnO_2 and cubic Mn_2O_3 as shown in Fig. 1(b). The existence of the two phases in Fig. 1(b) was understood that the manganese oxides undergo structural and compositional changes as elevated temperatures ($T \sim 400$ °C) [20]. For example, γ-MnO_2 is decomposes to Mn_2O_3 at $T > 450$ °C [21]. Although any phases

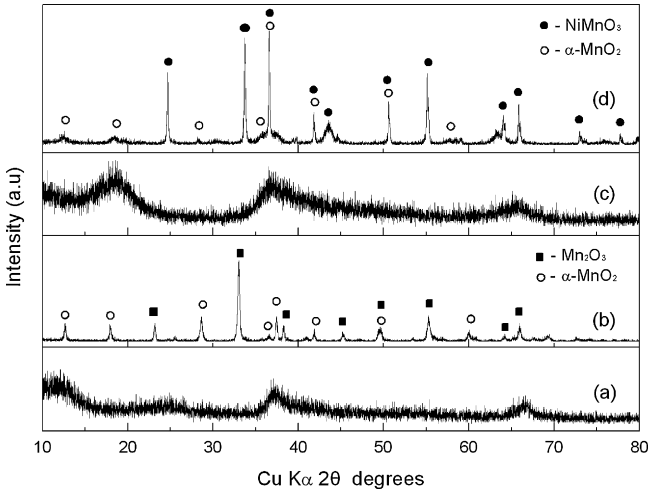

Fig. 1. The X-ray power diffraction patterns of the samples: (a) as-prepared sample A; (b) after firing the sample A at 500 °C for 6 h; (c) as-prepared sample B; (d) after firing the sample B at 500 °C for 6 h.

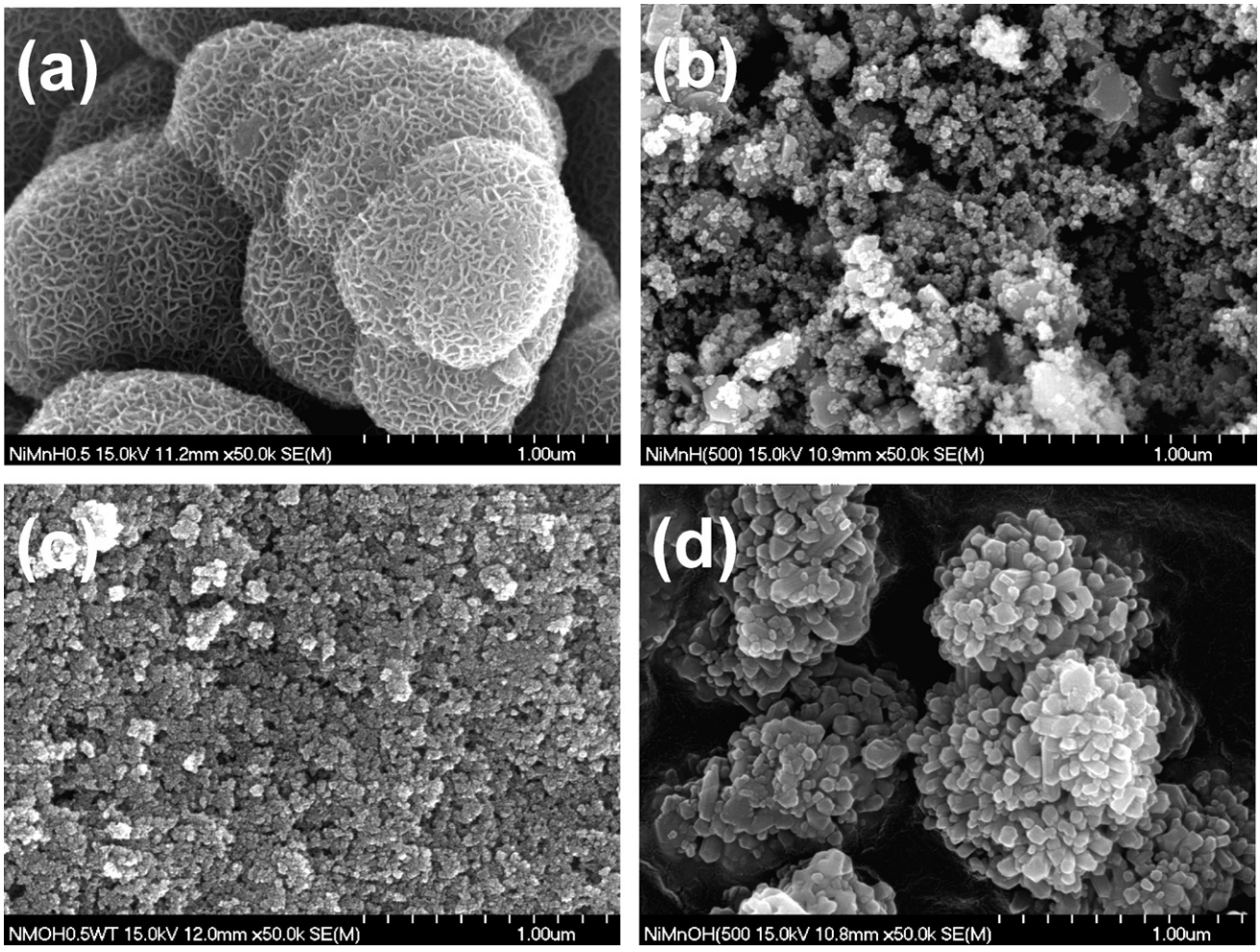

Fig. 2. The Field Emission SEM micrograph of the samples of: (a) as-prepared sample A; (b) after firing sample A at 500 °C for 6 h; (c) as-prepared sample B; (d) after firing sample B at 500 °C for 6 h.

related to nickel was not found by X-ray diffraction patterns, the result of ICP shows the small amount of nickel was contained in the as-prepared sample A (Table 1). Also, the X-ray patterns of the fired sample B show the existence of the two phases corresponding to tetragonal α-MnO_2 and Rhomboheral $NiMnO_3$ as shown in Fig. 1(d).

Fig. 2 shows the FESEM micrographs revealing the morphology of the samples. While the FESEM micrograph of the as-prepared sample A shows that the as-prepared sample A is in the form of spherical agglomerates, approximately 0.8–1.0 μm in diameter, the sample A obtained by firing at 500 °C for 6 h has the smaller primary particles (<30 nm) with narrow particle size distribution as shown in Fig. 2(a) and (b). The as-prepared sample A exhibits loosely bonded agglomerates with very weak inter-particle bonding forces so that it readily decomposes to individual nanoparticles once enough activating treatments are induced. The FESEM micrograph of the as-prepared sample B shows that the average particle size was approximately 15 nm in diameter with uniform particle size distribution as shown in Fig. 2(c). Firing this sample B at 500 °C for 6 h causes the size of original primary particles increase to about 100 nm as shown in Fig. 2(d).

Fig. 3 shows the X-ray powder diffraction patterns, the Rietveld refinement result for the X-ray powder diffraction patterns and the FESEM micrograph of the lithiated sample A ($Li_{1.296}Ni_{0.056}Mn_{0.648}O_2$) prepared by quenching at 800 °C. The X-ray diffraction patterns of $Li_{1.296}Ni_{0.056}Mn_{0.648}O_2$ were indexed a layered structure based on hexagonal α-$NaFeO_2$ (space group: *R*-3*m*, 166), except for broad peaks between 20° and 25° as shown in Fig. 3(a) and (b). These broad peaks indicate the short-ranged superstructure ordering of the Li, Ni, and Mn atoms in the transition metal layers and indicating the presence of monoclinic Li_2MnO_3 phase [13,22]. If the lithium and manganese ions in the transition metal layers are partially disordered by nickel ions, superstructure peaks will be shown as broad buckle. Table 2 shows the structural parameters determined by Rietveld refinement for the lithiated sample A ($Li_{1.296}Ni_{0.056}Mn_{0.648}O_2$). The Rietveld refinement result shows that the reliability values is relatively high because the X-ray powder diffraction patterns have the broad peaks and the maximum intensity is very low as shown in Fig. 3(b) and Table 2. The sample shows 4.99 of a trigonal distortion value of *c*/*a* ratio of 4.99, which indicates that it os ordered layered materials. A 4.90 corresponds to cubic lattice constants

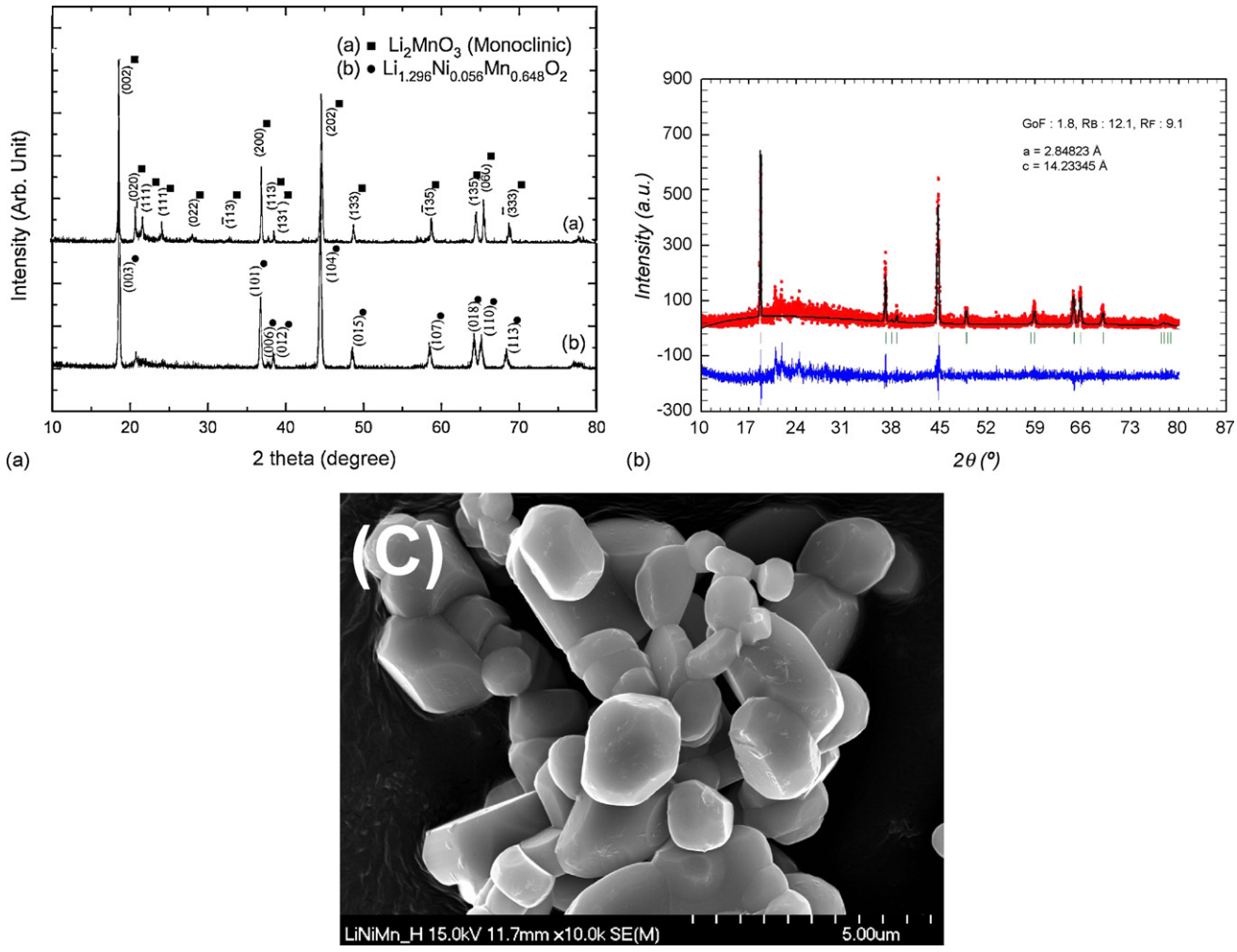

Fig. 3. (a) The X-ray powder diffraction patterns; (b) the Rietveld refinement result for the X-ray powder diffraction patterns; (c) the FESEM micrograph of the lithiated sample A ($Li_{1.296}Ni_{0.056}Mn_{0.648}O_2$) prepared by quenching at 800 °C.

and *c*/*a* ratio of well-layered $LiCoO_2$ is 4.99. Also the clear splitting between the (0 1 8)/(1 1 0) peaks indicates that all the prepared samples have a well-defined layered structure. In fact, the $Li_{1.296}Ni_{0.056}Mn_{0.648}O_2$ ($Li_{1.944}Ni_{0.056}Mn_{0.972}O_3$) material has a very small amount of Ni with similar chemical composition to Li_2MnO_3 suggesting that it might have monoclinic and rhombohedral crystallographic characteristics simultaneously. Both of monoclinic and rhombohedral structures holding the plane of closely packed oxygen exhibit a similar X-ray diffraction pattern such as (0 0 2), (2 0 2) planes of monoclinic structure overlapped to the (0 0 3), (1 0 4) planes of rhombohedral structure, respectively, since lithium and oxygen layers in the monoclinic structure shows almost exactly same packing sequence as rhombohedral structure except a transition metal layer. The morphology of the lithiated sample A together with XRD results reveals that the particles are well crystallized. The particles of the lithiated sample A ($Li_{1.296}Ni_{0.056}Mn_{0.648}O_2$) shows non-agglomerated primary particles with approximately 2–3 μm in size as shown in Fig. 3(c). It has been reported that manganese oxide has a substantially tendency for crystal growth with respect to a solid-state reaction at high temperature [23] resulting much larger particles than the samples heated at 500 °C as shown in Fig. 2.

Table 2
The Rietveld fit results of the lithiated sample A ($Li_{1.296}Ni_{0.056}Mn_{0.648}O_2$) prepared by quenching at 800 °C

a (Å)	2.848
c (Å)	14.233
c/*a*	4.997
RB (%)	12.1
RF (%)	9.1
GoF	1.8

Fig. 4 shows the charge–discharge curves of the lithiated sample A in the voltage range of 2.0–4.8 V at a current density of 0.2 mA cm^{-2}. It reveals that the voltage profile of the first charge cycle is very different from the others. There is a plateau at about 4.5 V during the first charge that leads to an increase in reversible capacity. Lu et al. reported that the voltage profile of the first charge up to 4.45 V is attributed to extraction of lithium by oxidation of Ni^{2+} to Ni^{4+}. The plateau at 4.5 V is related to the extraction of the remaining lithium from the lithium layer with accompanying the oxygen loss [14]. Recently, Shin et al. reported that, if Li^+ ions could be

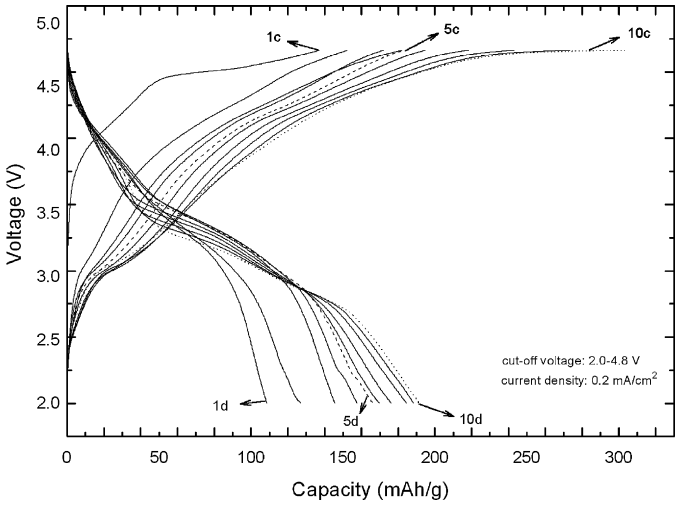

Fig. 4. Charge–discharge curves of Li/Li-inserted sample A ($Li_{1.296}Ni_{0.056}Mn_{0.648}O_2$) cell in the voltage range of 2.0–4.8 V at a current density of 0.2 mA cm^{-2}.

removed from the host structure, Mn^{4+}-based samples could show a capacity by the hybridization of $O2^-$:2p and $Mn^{4+/5+}$:3d at higher voltage (>4.5 V) [24]. There is a irreversible capacity of about 30 mAh g^{-2} during the first charge–discharge as shown in Fig. 4. The electrochemical performance of the lithiated sample A ($Li_{1.296}Ni_{0.056}Mn_{0.648}O_2$) shows the very interesting results that the discharge capacity continuously increases upon 1st to 10th cycles. The lithiated sample A ($Li_{1.296}Ni_{0.056}Mn_{0.648}O_2$) exhibits a discharge capacity of 108 mAh g^{-2} at 1st cycle and a larger discharge capacity of 192 mAh g^{-2} at 10th cycle.

Fig. 5 shows the differential capacity vs. voltage of Li/Li-inserted sample A ($Li_{1.296}Ni_{0.056}Mn_{0.648}O_2$) cell in the voltage range of 2.0–4.8 V at a current density of 0.2 mA cm^{-2}. The peak at 3.3 V separates into two peaks (2.8, 3.3 V) after fifth cycle shown in Fig. 5. Since Mn^{4+} (Li_2MnO_3), which was designed as framework reduced to Mn^{3+} due to oxidation of the oxygen ion in the crystal structure

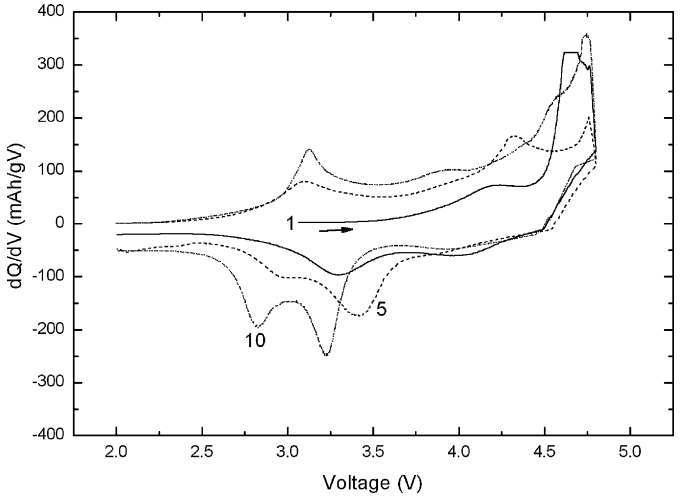

Fig. 5. The differential capacity vs. voltage of Li/Li-inserted sample A ($Li_{1.296}Ni_{0.056}Mn_{0.648}O_2$) cell in the voltage range of 2.0–4.8 V at a current density of 0.2 mA cm^{-2}.

($O^{2-+\delta} + Mn^{4+} \rightarrow O^{2-} + Mn^{4+} - 1/4\delta Mn^{4+} + 1/3\delta Mn^{3+}$) [25], two distinct plateaus might be shown at 3.3, 2.8 V indicating the transformation to a spinel structure happens. Lu et al. reported that all the Ni is reduced to Ni^{2+} once the cells reach 3.5 V and Mn reduces continuously until the Li layers are occupied again below 3.5 V [14]. Nahm et al. reported that in the case of Ni-doped $Li_{0.7}[Li_{1/12}Ni_{1/12}Mn_{5/6}]O_2$ the transition of Mn^{4+} to Mn^{3+} will begin after all Ni^{4+} are totally reduced into Ni^{2+} during the charge process. This phenomenon is able to reduce the rapid capacity fading induced during the charge/discharge processes [26]. However, since $Li_{1.296}Ni_{0.056}Mn_{0.648}O_2$ material contains negligible amounts of nickel, it is unreasonable to consider any redox couples related to nickel for contributing the capacities at 2.8 and 3.3 V. Rather, it is assumed that both of the capacities at 3.3 and 2.8 V may be attributed to Mn^{3+}/Mn^{4+} redox couple arising from Li insertion to tetrahedral and octahedral site in the materials, which is partially transformed to spinel structures in discharging reactions. Therefore, the small amounts of Ni in the sample seems act as defects in Li_2MnO_3 to facilitate electrochemical reaction of Li_2MnO_3-like compound [16–19]. The lattice energies in specific sites, which directly affect work function values, are influenced by several factors such as Madelung constants, polarization effects, crystal field stabilization energy, etc. It is hard to state clearly at this stage regarding the origin of the capacities at 3.3 and 2.8 V. Therefore, a further study is necessary to understand the relationship between the potential and the material's structural information while cycling. The curve also shows that the peak indicated the Li_2O extraction at higher voltage (>4 V) remains on cycling. This suggests that the continuous increase of capacity may be attributed to the remaining Li_2O after cycling. Shin et al. reported that the sufficient electrochemical inactive Li_2MnO_3 component contributes to stabilization of the Li–Ni–Mn–O structures. The discharge capacities of the $Li[Ni_xLi_{(1/3-2x/3)}Mn_{(2/3-x/3)}]O_2$ electrodes increase when the nickel content is small ($x \leq 0.275$), and then stabilize within about 20th cycles [15]. The increase of the peak height during cycling may be attributed to an increase in electrical contact between the particles of the cathode material [27]. Both the negative shift of the reduction peaks and the positive shift of the oxidation peaks seem to related to the increase of the cell resistance.

4. Conclusions

The nickel–manganese compounds were synthesized by redox reactions in aqueous solutions at room temperature in two different conditions (adding HCl or adding KOH). The selected as-prepared sample obtained by adding HCl was developed as a precursor for electrode materials to examine the electrochemical activity of Li_2MnO_3-like $Li_{1.296}Ni_{0.056}Mn_{0.648}O_2$. X-ray diffraction patterns of the lithiated sample A ($Li_{1.296}Ni_{0.056}Mn_{0.648}O_2$) was indexed to a layered structure based on hexagonal α-$NaFeO_2$ with signs of superstructure existence indicating of monoclinic Li_2MnO_3 phase. The initial discharge capacity of the lithiated

sample A ($Li_{1.296}Ni_{0.056}Mn_{0.648}O_2$) continuously increases during electrochemical cycling. The lithiated sample A ($Li_{1.296}Ni_{0.056}Mn_{0.648}O_2$) exhibits the maximum discharge capacity of 192 mAh g^{-1} on 10th cycle between 2.0 and 4.8 V at a current density of 0.2 mA cm^{-2}. Further study on the synthesis of nickel–manganese nanoparticles in optimized process conditions for precursor materials is being undertaken.

Acknowledgements

This research was supported by the Program for the Training of Graduate Students in Regional Innovation which was conducted by the Ministry of Commerce, Industry and Energy of the Korean Government.

References

[1] (a) F.J. Disalvo, Science 247 (1990) 649;
(b) J.B. Wiley, R.B. Kaner, Science 255 (1992) 1093;
(c) A. Stein, S.W. Keller, T.E. Mallouk, Science 259 (1993) 1558.
[2] A. Manthiram, J. Kim, Chem. Mater. 10 (1998) 2895.
[3] J. Livage, M. Henry, C. Sanchez, Prog. Solid State Chem. 18 (1988) 259.
[4] A. Manthiram, J.B. Goodenough, Nature 329 (1987) 701.
[5] Y.F. Shen, R.P. Zerger, R.N. DeGuzman, S.L. Suib, L. Mccurdy, D.I. Potter, C.L. O'Young, Science 260 (1993) 511.
[6] R.J. Gummow, M.M. Thackeray, J. Electrochem. Soc. 140 (1993) 3365.
[7] Y. Shao-Horn, S.A. Hackeray, J. Electrochem. Soc. 146 (1999) 2404.
[8] Y.I. Jang, B. Huang, Y.M. Chiang, D.R. Sadoway, Electrochem. Solid-State Lett. 1 (1998) 13.
[9] Z.H. Lu, J.R. Dahn, J. Electrochem. Soc. 149 (2002) 815.
[10] Y. Shao-Horn, S.A. Hackney, A.R. Armstrony, P.G. Bruce, R. Gitzendanner, C.S. Johnson, M.M. Thackeray, J. Electrochem. Soc. 146 (2404) 2404.
[11] K. Numata, C. Sakaki, S. Yamanaka, Solid State Ionics 117 (1999) 257.
[12] T. Ohzuku, Y. Makimura, Chem. Lett. (2001) 744.
[13] Z. Lu, D.D. MacNeil, J.R. Dhan, Electrochem. Solid-State Lett. 4 (11) (2001) 191.
[14] Z. Lu, L.Y. Beaulieu, R.A. Donaberger, C.L. Thomas, J.R. Dhan, J. Electrochem. Soc. 149 (2002) A778.
[15] S.-S. Shin, Y.-K. Sun, K. Amine, J. Power Sources 112 (2002) 634.
[16] A.D. Robertson, P.G. Bruce, Chem. Commun. 23 (2002) 2790.
[17] P. Kalyani, S. chitra, T. Mohan, S.J. Gopukumar, J. Power Sources 80 (1999) 103.
[18] C.S. Johnson, J.-S. Kim, C. Lefief, N. Li, J.T. Vaughey, M.M. Thackeray, Electrochem. Comm. 6 (2004) 1085.
[19] C.S. Johnson, N. Li, J.T. Vaughey, S.A. Hackney, M.M. Thackeray, Electrochem. Comm. 7 (2005) 528.
[20] H. Ikeda, US Patent 4. 133 856.
[21] C. Tsang, J. Kim, A. Manthiram, J. Solid State Chem. 137 (1998) 28.
[22] K.S. Kim, S.W. Lee, H.S. Moon, H.J. Kim, B.W. Cho, W.I. Cho, J.B. Choi, J.W. Park, J. Power Source (2004).
[23] Z.P. Guo, S. Zhong, G.X. Wang, G. Walter, H.K. Liu, S.X. Dou, J. Electrochem. Soc. 149 (2002) A792.
[24] Y. Shin, A. Manthiram, Electrochim. Acta 48 (2003) 3583.
[25] Y.K. Sun, M.G. Kim, S.H. Kang, K. Amine, J. Mater. Chem. 13 (2003) 319.
[26] K.S. Park, M.H. Cho, S.J. Jin, C.H. Song, K.S. Nahm, Korean J. Chem. Eng. 21 (2004) 983.
[27] X. Wu, K.S. Ryu, Y.S. Hong, Y.J. Park, S.H. Chang, J. Power Source 132 (2004) 219.